Journal of Materials Chemistry C

PAPER

View Article Online
View Journal | View Issue

Cite this: J. Mater. Chem. C, 2014, 2, 9689

Realization of a self-powered ZnO MSM UV photodetector with high responsivity using an asymmetric pair of Au electrodes†

Hong-Yu Chen,[abc] Ke-Wei Liu,*[a] Xing Chen,[a] Zhen-Zhong Zhang,[a] Ming-Ming Fan,[ab] Ming-Ming Jiang,[a] Xiu-Hua Xie,[ab] Hai-Feng Zhao[a] and De-Zhen Shen*[a]

Received 18th August 2014
Accepted 15th September 2014

DOI: 10.1039/c4tc01839g

www.rsc.org/MaterialsC

We demonstrate a novel type of ZnO self-powered photodetector based on the asymmetric metal-semiconductor-metal (MSM) structure: one Au interdigitated electrode with wide fingers and the other one with narrow fingers. These ZnO photodetectors exhibit attractive photovoltaic characteristics at 0 V bias. More interestingly, with increasing the asymmetric ratio (the width of wide fingers : the width of narrow fingers) of the interdigitated electrodes, the responsivity of the ZnO self-powered UV photodetectors was enhanced obviously, reaching as high as 20 mA W^{-1} when the asymmetric ratio was 20 : 1. A physical model based on band energy theory was developed to illustrate the origin of the photoresponse at 0 V in our device. Our findings provide a new route to realizing self-powered photodetectors.

Introduction

Ultraviolet photodetectors have drawn extensive attention due to their broad applications including missile plume sensing, flame detection, converting space-to-space communication, and water purification, *etc.*[1–6] From an application point of view, UV photodetectors operating without any power supply, namely self-powered photodetectors, have some special advantages, such as saving energy, small device size and suitable use in extreme conditions. Thus, self-powered UV photodetectors have recently received increasing attention. Till now, p–n junctions, Schottky junctions, and heterojunctions have been widely used to realize these types of devices due to their efficient separation ability of photo-excited electron–hole pairs by the photovoltaic effect.[7–15]

In the past several decades, ZnO has been investigated for use in photodetectors in the UV range due to its wide direct band gap (~3.37 eV), low defect density, and strong radiation hardness.[4,5,16,17] However, owing to the lack of high quality and stable p-ZnO, very little information is available regarding ZnO p–n homojunction photodiodes. Although some self-powered ZnO UV photodetectors have been demonstrated based on vertical Schottky junctions and heterojunctions, many problems still exist in these devices, such as the complicated preparation process and the poor electrode contacts in vertical Schottky photodiodes. As for heterojunctions, the large lattice mismatch between ZnO and other materials could strongly degrade the device performance. Therefore, the existing self-powered ZnO photodetectors usually have a poor performance, and a new type of self-powered UV photodetector with high responsivity is urgently needed.

Till now, most ZnO-based photodetectors are based on the metal-semiconductor-metal (MSM) structures, which are controllable, stable, and can be fabricated easily. However, the traditional MSM photodetectors always require an external power source as the driving force to generate photocurrent due to their two symmetric Schottky contacts connected back-to-back on a planar surface.[4,18–22] According to the previous reports, MSM devices using different materials as the two electrodes (one is an Ohmic contact and the other is a Schottky contact) were recognized as planar Schottky photodiodes, which can be operated at 0 V bias.[23] However, just like the vertical Schottky photodetector, the fabrication process of MSM devices with two different electrode materials is complex, and their performance is still not very high. Recently, it was found that the size of metal electrodes can strongly affect the distribution of the electric field built in the Schottky junction.[24–27] As is well known, the electric field can prevent the recombination of photo-generated electron–hole pairs, and efficiently separate the photo-generated carriers. Therefore, self-powered ZnO MSM photodetectors are expected to be realized by using an asymmetric pair of planar electrodes.

[a]State Key Laboratory of Luminescence and Applications, Changchun Institute of Optics, Fine Mechanics and Physics, Chinese Academy of Sciences, Dongnanhu Road 3888, Changchun, 130033, People's Republic of China. E-mail: Liukw@ciomp.ac.cn; shendz@ciomp.ac.cn

[b]Graduate University of the Chinese Academy of Sciences, Beijing, 100049, People's Republic of China

[c]Department of Materials Science, Fudan University, Shanghai, 200433, People's Republic of China

† Electronic supplementary information (ESI) available. See DOI: 10.1039/c4tc01839g

In this article, we demonstrated a novel ZnO self-powered UV photodetector with the asymmetric MSM structure: one Au interdigitated electrode with wide fingers and the other one with narrow fingers. Interestingly, once the finger width of the wide electrode is fixed, the responsivity could be significantly enhanced by decreasing the finger width of the narrow electrode. The responsivity at a wavelength of 365 nm without any external power supply can reach as high as 20 mA W^{-1} and this value is higher than that of previously reported ZnO-based self-powered photodetectors.[8,28–31] A physical model based on band energy theory was developed to illustrate the origin of the photoresponse at 0 V in our ZnO self-powered photodetectors.

Experimental section

In order to fabricate the self-powered ZnO detector, ZnO layers were employed as the active layers of the detector, and they were grown on an *a*-plane sapphire substrate in a VG V80H plasma-assisted molecular-beam epitaxy (MBE) system. Prior to growth, the sapphire substrate was pretreated at 800 °C for 30 min to remove any possibly adsorbed contaminants and produce a clean surface. High-purity (6 N) elemental zinc was used as the precursor for growth, and the oxygen source used was radical oxygen produced in a plasma cell operating at 300 W. The pressure in the growth chamber during growth was fixed at 2×10^{-3} Pa. Firstly, ZnO buffer layers were deposited onto the *a*-plane sapphire substrate at 400 °C for 6 min, and then at 750 °C for 120 min, after which ~500 nm ZnO layers were epitaxied. After that, the asymmetric Au interdigital electrodes were patterned using a photolithography process.

The structure and morphology of the ZnO films were characterized by scanning electron microscopy (SEM; Hitachi, S-4800), atomic force microscopy (AFM; Bruker, MultiMode-8) and X-ray diffraction (Bruker, D8X). A Hall measurement system (Lake Shore, HMS7707) and a Keithley 2611A Source Meter were employed to investigate the electrical properties. The spectral response and the time resolved response of the photodetector were measured by a 150 W Xe lamp, monochromator, chopper, lock-in amplifier, and a YAG:Nd laser (266 nm), respectively.

Results and discussion

Fig. 1(a) shows the SEM image of the as-grown ZnO film, and the inset is the high-resolution picture. It can be found that the ZnO film is uniformly fabricated on the *a*-plane sapphire with a relatively smooth surface. To further investigate the surface properties of the ZnO film, the topographies of the ZnO epilayer were characterized by typical tapping-mode AFM. As shown in Fig. 1(b), the average rms roughness of the ZnO film is calculated to be ~2.8 nm. The structural characterizations of the ZnO films were assessed by X-ray diffraction (XRD) [see Fig. 1(c)]. Besides the diffraction from the substrate, only one peak at 34.44° can be observed from the XRD pattern, which can be indexed to the diffraction from the (0002) facet of wurtzite ZnO. The XRD result indicates that the ZnO layer has crystallized in a hexagonal wurtzite structure with *c*-axis preferred orientation. The X-ray rocking curve of the ZnO film is displayed in the inset

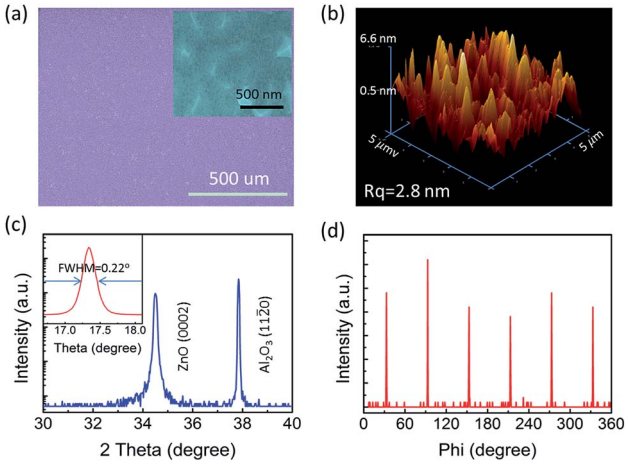

Fig. 1 (a) Low and high magnification SEM, and (b) AFM images of the ZnO film. (c) XRD pattern of the ZnO film. The inset shows its X-ray rocking curve. (d) X-ray phi-scan spectrum of the ZnO film.

of Fig. 1(c), and a Gaussian lineshape with a full width at half maximum (FWHM) of around 0.22° can be observed. In addition, the phi-scan was employed to further analyse the in-plane orientation of the ZnO film, as shown in Fig. 1(d). Six sharp phi-scan peaks of the ZnO at 60° intervals confirm that the epitaxial ZnO exhibits a single-domain wurtzite structure with hexagonal symmetry.

Fig. 2 is the schematic illustration of ZnO MSM UV photodetectors based on the above mentioned films. 12 pairs of interdigital metal electrodes with 500 μm length and 10 μm gap were formed by a 40 nm thick Au layer. In order to investigate the size effect of metal electrodes on the performance of the

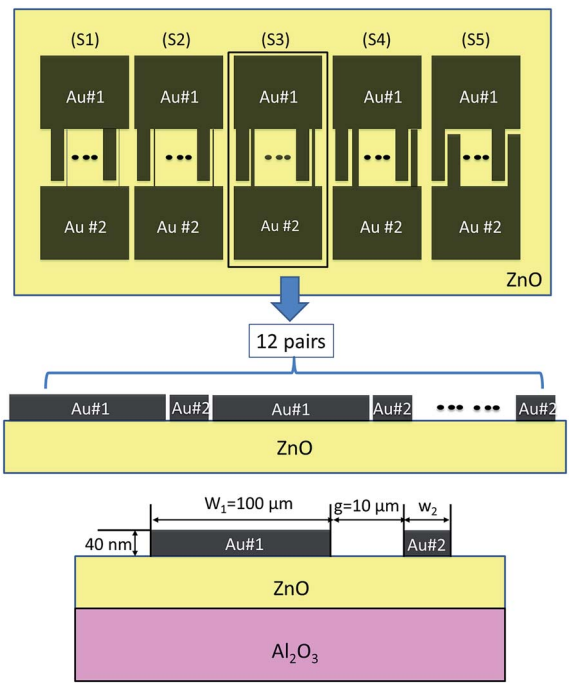

Fig. 2 Schematic illustration of the self-powered ZnO detector.

ZnO MSM photodetectors, one electrode (Au#1) finger width (w_1) was fixed at 100 μm, while the other electrode (Au#2) finger width (w_2) varies between 5 μm and 100 μm. The devices with w_2 of 5, 10, 25, 50, and 100 μm are labeled as S1, S2, S3, S4, and S5, respectively.

Fig. 3(a) shows the photoresponse spectra of the aforementioned 5 photodetectors at 0 V bias. It can be found that all of the detectors based on the asymmetric Au interdigitated electrodes structure exhibited an attractive photovoltaic characteristic. More interestingly, with the decrease in w_2 from 100 μm to 5 μm, the asymmetric ratio of the interdigitated electrodes ($w_1 : w_2$) increases from ~1 : 1 to 20 : 1 and the responsivity was enhanced significantly. For S1 (asymmetric ratio = 20 : 1), the maximum responsivity can reach as high as ~20 mA W^{-1}, which is the highest value ever reported for ZnO-based self-powered photodetectors, including p–n junctions, metal-oxide-semiconductor structures, Schottky junctions and heterojunctions (see Table 1). A sharp cut off of responsivity can be seen at a wavelength of ~375 nm, corresponding to the band gap energy of ZnO. In addition, the UV-visible rejection ratio [R (365 nm)/R (400 nm)] is more than 2 orders of magnitude. The sharp cut-off edge and the relatively high UV-visible rejection ratio at 0 V indicate that our device is a high-performance intrinsic visible-blind self-powered UV photodetector.

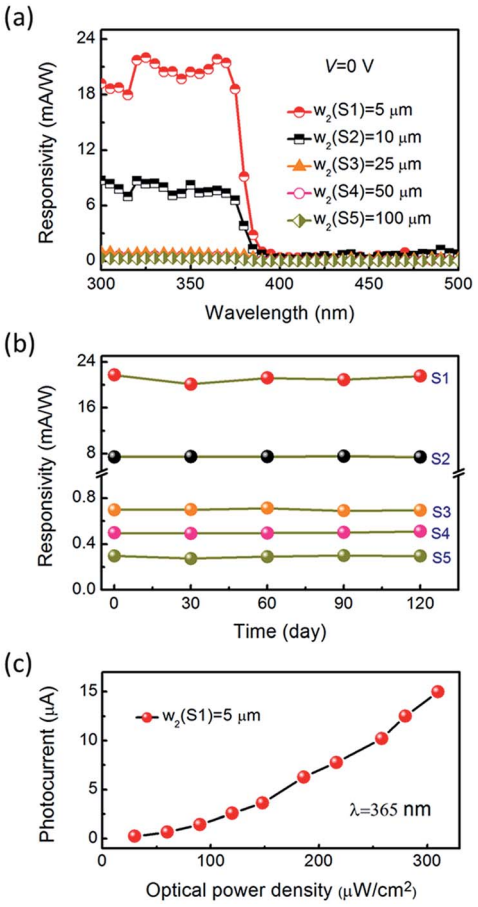

Fig. 3 (a) Spectral photoresponse of the ZnO photodetectors at 0 V bias. (b) The responsivity at 365 nm as a function of time. (c) Light-intensity dependence of the photocurrent at 365 nm.

As mentioned above, one advantage of self-powered devices is that they are suitable for long operation times in extreme conditions, and thus the reliability of these devices should be very important. As shown in Fig. 3(b), the responsivities of the detectors were nearly constant during the 120 days, indicating the high reliability and stability of our self-powered photodetectors. To further characterize our photodetector, the illumination intensity-dependence of the photocurrent was measured under a UV light (365 nm). In Fig. 3(c), as the illumination intensity increases from 30 μW cm^{-2} to 310 μW cm^{-2}, the photocurrent increases nonlinearly, suggesting a complex process of electron–hole generation, recombination, and trapping in our device.

The temporal photoresponse of the ZnO self-powered UV photodetector (S1) was measured at 0 V with a pulsed YAG:Nd laser as the optical source (the laser pulse width was 10 ns and the frequency was 10 Hz), and the measurement setup is shown in Fig. S1.† As shown in Fig. 4(a), the photoresponse of our self-powered device was very fast, highly stable and reproducible. The 10–90% response time (τ_r) and decay time (τ_d) were measured to be ~710 ns and ~4 μs, respectively [see Fig. 4(b)]. In addition, considering the negative photo-induced voltage and the measurement configuration, the potential of Au#1 is higher than that of Au#2 under UV illumination for S1.

To explore the origin of such an attractive photovoltaic characteristic in these detectors, I–V characteristics measurements were carried out on the asymmetric MSM (Au#1–ZnO–Au#2) detectors. The left image in Fig. 5(a) shows the schematic illustration of the configuration for measuring the I–V characteristics and the image on the right is the optical image of the five devices fabricated on one large ZnO film. As illustrated in Fig. 5(b), the contact between Au and ZnO is a typical Schottky contact for all devices. Moreover, with decreasing w_2 from 100 μm to 5 μm, the transition from a symmetric to an asymmetric profile of the I–V curves can be observed between the positive and negative voltage regions. In general, for a Schottky contact, if $E_{00} \ll k_BT$, the thermionic emission is dominated in the junction electronic transport process without tunneling, where k_B is the Boltzmann constant, T is the absolute temperature, and E_{00} is the characteristic energy related to the tunneling probability.[32–35] E_{00} can be expressed by the following formula:

$$E_{00} = (q\hbar/2)(N/m^*\varepsilon_s)^{1/2} \quad (1)$$

where q is the elementary charge, $\hbar$ is the reduced Planck constant, N is the carrier density, m^* is the effective mass and ε_s is the relative dielectric permittivity. In this work, $m_e = 0.27m_0$, and $\varepsilon_s = 8.3$ for ZnO, and the carrier concentration N is about 9.3×10^{16} cm^{-3}. E_{00} is about 2.2 meV for the ZnO films, which is much smaller than the thermal energy k_BT at room temperature (26 meV). Thus, the current passing through the Schottky barrier can be described as follows:

$$I = I_0 \exp(qV/nK_BT)[1 - \exp(-qV/k_BT)] \quad (2)$$

Table 1 Comparison of the characteristic parameters of the ZnO-based self-powered photodetectors obtained in the present and previous work

Devices	Materials and structures	Responsivity at 0 V bias (mA W^{-1})	UV-visible rejection ratio	Ref.
Asymmetric MSM	Au#1–ZnO–Au#2	20	10^2	This work
p–n junction	p-ZnO(Li,N)/n-ZnO	0.018	—	28
Heterojunction	p-GaN/n-ZnO	0.001	10	8
MS	Au/MgZnO	0.059	$<10^2$	29
MIS	Au–ZnO(i)/ZnO(n)/In	0.03	—	30
MOS	Au/MgO/MgZnO	11	—	31

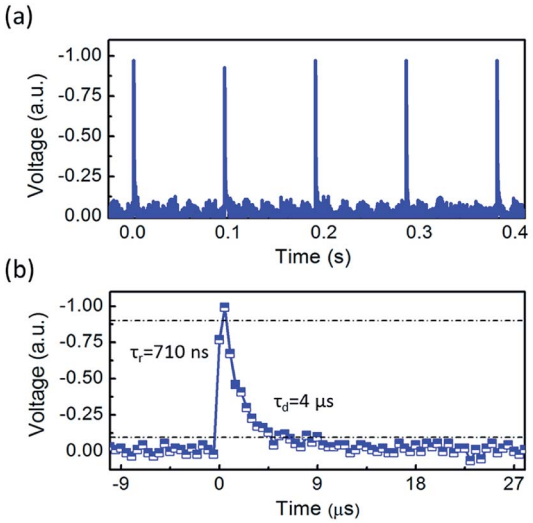

Fig. 4 (a) and (b) Time-resolved response of the photovoltage of device S1 at the applied bias of 0 V.

$$I_0 = AA^* \exp(-q\varphi_B/k_B T) \quad (3)$$

where k_B is the Boltzmann constant, T is the absolute temperature, n is the ideality factor, A is the junction area, A^* is the Richardson constant ($A^* \equiv 4\pi m^* q^2/h^3$), φ_B is the barrier height, h is the Planck constant, and I_0 is the reverse saturation current. Based on the thermionic model, I_0 could be derived from the I–V curves of the photodetectors in Fig. 4(b). From calculations using eqn (2) and (3), it can be concluded that the Schottky barrier height in all devices is around 0.8 eV. This means that the Schottky barrier between Au and ZnO is independent of the size of the electrodes. The reason for this phenomenon is that the Schottky contact between Au and ZnO is determined by their work function and interface states.[36]

In order to better understand the mechanism of the photoresponse at 0 V of our devices, a model based on energy band theory was proposed as shown in Fig. 6. Schematics of the energy band diagrams in the dark and under UV illumination are displayed in Fig. 6(a) and (b), respectively. In the dark, Schottky barriers with a barrier height of ~0.8 eV are formed at the Au#1–ZnO and Au#2–ZnO interfaces, where the Au electrodes and ZnO have the same Fermi energy level (EF). According to the theory calculations (ref. 24–26 and Fig. S2†),

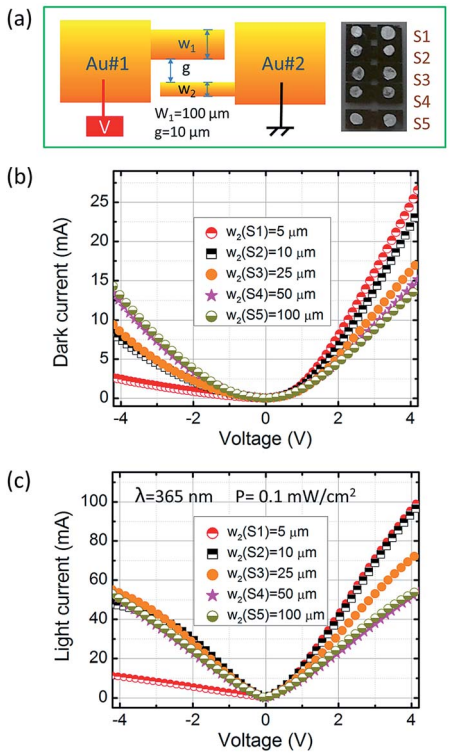

Fig. 5 (a) Schematic illustration of the configuration for measuring the I–V characteristics (left) and optical image of the devices (right). (b) I–V characteristics of the asymmetric MSM (Au#1–ZnO–Au#2) photodetectors in the dark. (c) I–V characteristics of the photodetectors under UV illumination at a wavelength of 365 nm.

the width of the depletion region at the Au#1–ZnO interface should be larger than that at the Au#2–ZnO interface [see Fig. 6(a)]. Under UV illumination, electron–hole pairs are generated in ZnO as shown in Fig. 6(b). The generated electrons in the conduction band (CB) tend to move away from the contact, while the holes in the valence band (VB) tend to move close to the interface toward the metal side. The accumulated and trapped holes at the interfaces modify the local potential profile, so that the effective height of the Schottky barriers is lowered.[37–39] Due to the difference in the width of the depletion layer between Au#1–ZnO and Au#2–ZnO, the asymmetric electric potential distribution in the ZnO film could induce the

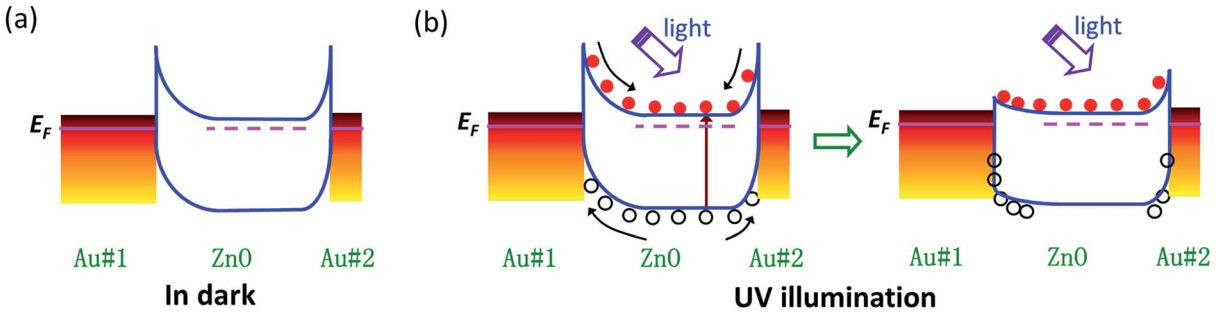

Fig. 6 Energy band diagrams of the asymmetric MSM photodetector at 0 V in the dark (a) and under UV light (b).

difference in the carrier separation and transport. Thus, the number of accumulated and trapped holes at the two interfaces is different, which induces the difference in the decrease of the Schottky barrier height between Au#1–ZnO and Au#2–ZnO. As a result, a typical photovoltaic characteristic can be observed in the asymmetric MSM photodetectors at 0 V bias voltage. It must be mentioned here that the barrier height change is strongly dependent on the electrical properties of ZnO and the structure of the Au electrodes, which could determine the direction of photovoltage. As for traditional MSM photodetectors, the structure of two symmetric electrodes can not produce any photoresponse without a power supply.[4,7,17,20,22,32,40] It is worth mentioning that S5 with the symmetric interdigital electrodes also shows a responsivity at 0 V in our experiment, which is mainly caused by experimental errors (see Fig. S3†).

Conclusions

In summary, the self-powered ZnO UV photodetectors were firstly realized by using the asymmetric pair of planar electrodes. The responsivity at 0 V was significantly enhanced by increasing the asymmetric ratio between the two electrodes, and could reach as high as 20 mA W^{-1} with an asymmetric ratio of 20 : 1. This value is higher than that of other kinds of self-powered ZnO-based photodetectors such as p–n junctions, Schottky junctions, and heterojunctions. The origin of the photoresponse at 0 V in our devices should be associated with the asymmetric electric potential distribution in ZnO films and the accumulated and trapped holes at the Au/ZnO interfaces. In addition, due to its advantage of relatively simpler fabrication technology, this asymmetric MSM structure should be an excellent choice for obtaining high-efficiency self-powered ZnO UV photodetectors, and this method can also be extended to devices based on other semiconductor materials.

Acknowledgements

The authors thank Dr Jian-Wei Zhang and Dr Deng-Kui Wang for their technical assistance and kind help. This work is supported by the National Basic Research Program of China (973 program) (no. 2011CB302006), the National Natural Science Foundation of China (no. 10974197, 61475153, 11174273, 11104265, 11134009, 61376054), and the 100 Talents Program of the Chinese Academy of Sciences.

References

1 Z. Xu and B. M. Sadler, *IEEE Comm. Mag.*, 2008, **46**, 67–73.
2 Y. Taniyasu, M. Kasu and T. Makimoto, *Nature*, 2006, **441**, 325–328.
3 E. Gorokhov, A. Magunov, V. Feshchenko and A. Altukhov, *Instrum. Exp. Tech.*, 2008, **51**, 280–283.
4 L. Wang, Z. Ju, J. Zhang, J. Zheng, D. Shen, B. Yao, D. Zhao, Z. Zhang, B. Li and C. Shan, *Appl. Phys. Lett.*, 2009, **95**, 131113.
5 K. Liu, M. Sakurai and M. Aono, *Sensors*, 2010, **10**, 8604–8634.
6 G. Parish, S. Keller, P. Kozodoy, J. Ibbetson, H. Marchand, P. Fini, S. Fleischer, S. DenBaars, U. Mishra and E. Tarsa, *Appl. Phys. Lett.*, 1999, **75**, 247–249.
7 K. Liu, D. Shen, C. Shan, J. Zhang, B. Yao, D. Zhao, Y. Lu and X. Fan, *Appl. Phys. Lett.*, 2007, **91**, 201106.
8 H. Zhu, C. Shan, B. Yao, B. Li, J. Zhang, D. Zhao, D. Shen and X. Fan, *J. Phys. Chem. C*, 2008, **112**, 20546–20548.
9 Y.-Q. Bie, Z.-M. Liao, H.-Z. Zhang, G.-R. Li, Y. Ye, Y.-B. Zhou, J. Xu, Z.-X. Qin, L. Dai and D.-P. Yu, *Adv. Mater.*, 2011, **23**, 649–653.
10 P. Shaikh, V. Thakare, D. J. Late and S. Ogale, *Nanoscale*, 2014, **6**, 3550–3556.
11 L. Mandal, N. S. Chaudhari and S. Ogale, *ACS Appl. Mater. Interfaces*, 2013, **5**, 9141–9147.
12 L.-H. Zeng, M.-Z. Wang, H. Hu, B. Nie, Y.-Q. Yu, C.-Y. Wu, L. Wang, J.-G. Hu, C. Xie, F.-X. Liang, *et al.*, *ACS Appl. Mater. Interfaces*, 2013, **5**, 9362–9366.
13 Z. Wang, S. Ran, B. Liu, D. Chen and G. Shen, *Nanoscale*, 2012, **4**, 3350–3358.
14 X. Li, C. Gao, H. Duan, B. Lu, X. Pan and E. Xie, *Nano Energy*, 2012, **1**, 640–645.
15 Y. Xie, L. Wei, G. Wei, Q. Li, D. Wang, Y. Chen, S. Yan, G. Liu, L. Mei and J. Jiao, *Nanoscale Res. Lett.*, 2013, **8**, 1–6.
16 S. M. Hatch, J. Briscoe and S. Dunn, *Adv. Mater.*, 2013, **25**, 867–871.
17 D. C. Look, *Mater. Sci. Eng., B*, 2001, **80**, 383–387.
18 Z. Ju, C. Shan, D. Jiang, J. Zhang, B. Yao, D. Zhao, D. Shen and X. Fan, *Appl. Phys. Lett.*, 2008, **93**, 173505.

19 D. Walker, E. Monroy, P. Kung, J. Wu, M. Hamilton, F. Sanchez, J. Diaz and M. Razeghi, *Appl. Phys. Lett.*, 1999, **74**, 762–764.
20 D. L. Rogers, *J. Lightwave Technol.*, 1991, **9**, 1635–1638.
21 D. Li, X. Sun, H. Song, Z. Li, Y. Chen, H. Jiang and G. Miao, *Adv. Mater.*, 2012, **24**, 845–849.
22 S. Han, Z. Zhang, J. Zhang, L. Wang, J. Zheng, H. Zhao, Y. Zhang, M. Jiang, S. Wang, D. Zhao, *et al.*, *Appl. Phys. Lett.*, 2011, **99**, 242105.
23 M. Liao, Y. Koide and J. Alvarez, *Appl. Phys. Lett.*, 2007, **90**, 123507.
24 J. Freeouf, T. Jackson, S. Laux and J. Woodall, *Appl. Phys. Lett.*, 1982, **40**, 634–636.
25 G. Smit, S. Rogge and T. Klapwijk, *Appl. Phys. Lett.*, 2002, **81**, 3852–3854.
26 C. Donolato, *J. Appl. Phys.*, 2004, **95**, 2184–2186.
27 V. P. Zhdanov and B. Kasemo, *Phys. E*, 2011, **43**, 1486–1489.
28 H. Shen, C. Shan, B. Li, B. Xuan and D. Shen, *Appl. Phys. Lett.*, 2013, **103**, 232112.
29 G. Tabares, A. Hierro, J. Ulloa, A. Guzman, E. Munoz, A. Nakamura, T. Hayashi and J. Temmyo, *Appl. Phys. Lett.*, 2010, **96**, 101112.
30 P.-N. Ni, C.-X. Shan, S.-P. Wang, B.-H. Li, Z.-Z. Zhang, D.-X. Zhao, L. Liu and D.-Z. Shen, *J. Phys. Chem. C*, 2011, **116**, 1350–1353.
31 H. Zhu, C. Shan, L. Wang, J. Zheng, J. Zhang, B. Yao and D. Shen, *J. Phys. Chem. C*, 2010, **114**, 7169–7172.
32 S. M. Sze, *Semiconductor devices: physics and technology*, John Wiley & Sons, 2008.
33 B. Nie, J.-G. Hu, L.-B. Luo, C. Xie, L.-H. Zeng, P. Lv, F.-Z. Li, J.-S. Jie, M. Feng, C.-Y. Wu, *et al.*, *Small*, 2013, **9**, 2872–2879.
34 J. Liu, C. Shan, B. Li, Z. Zhang, C. Yang, D. Shen and X. Fan, *Appl. Phys. Lett.*, 2010, **97**, 251102.
35 X. Xie, Z. Zhang, B. Li, S. Wang, M. Jiang, C. Shan, D. Zhao, H. Chen and D. Shen, *Opt. Express*, 2014, **22**, 246–253.
36 Z. Zhang and J. T. Yates Jr, *Chem. Rev.*, 2012, **112**, 5520–5551.
37 Z. L. Wang, *Adv. Mater.*, 2012, **24**, 4632–4646.
38 O. Katz, V. Garber, B. Meyler, G. Bahir and J. Salzman, *Appl. Phys. Lett.*, 2001, **79**, 1417–1419.
39 X. Xie, Z. Zhang, B. Li, S. Wang, M. Jiang, C. Shan, D. Zhao, H. Chen and D. Shen, *Appl. Phys. Lett.*, 2013, **102**, 231122.
40 Q. Zheng, F. Huang, K. Ding, J. Huang, D. Chen, Z. Zhan and Z. Lin, *Appl. Phys. Lett.*, 2011, **98**, 221112.